Dynamical Analysis of a Hydraulic Pressure Relief Valve

Gábor Licskó * Alan Champneys † Csaba Hős ‡

Abstract—**A mathematical model is derived that describes the dynamics of a single stage relief valve embedded within a simple hydraulic circuit. The aim is to capture the mechanisms of instability of such valves, taking into account both fluid compressibility and the chattering behaviour that can occur when the valve poppet impacts with its seat. The initial Hopf bifurcation causing oscillation is found to be either super- or sub-critical in different parameter regions. For flow speeds beyond the bifurcation, the valve starts to chatter, a motion that survives for a wide range of parameters, and can be either periodic or chaotic. This behaviour is explained using recent theory of nonsmooth dynamical systems, in particular an analysis of the grazing bifurcations that occur at the onset of impacting behaviour.**

Keywords: relief valve, chaos, grazing, piecewise-smooth

1 Introduction

Hydraulic and pneumatic circuits are known sometimes to show undesirable behaviour that is peculiar to nonlinear dynamical systems. The source of the nonlinearity is often backlash, dry friction, on-off switches or impacting components, whose behaviour is not well modelled by smooth evolution equations. There are by now countless examples of such nonsmooth nonlinear problems that engineers face when they design mechanical systems, see e.g. [2, 3, 16] and references therein. Avoiding chatter in hydraulic relief valves is a good example of such a problem.

Relief valves are widely used to limit pressure in hydraulic power transmission and control systems. There is a rich literature that describes their usage in hydraulic circuits and gives information on their design and application; see [1] for a brief overview, or [11, 14] for a more industrial perspective. There have been numerous documented industrial examples where these kinds of valves have been found to vibrate when their equilibria lose stability, and many researchers have been interested in the investigation of this phenomenon. As far back as the 1960s researchers suspected that the piping to and from the relief valve cannot be neglected. Kasai [10] carried out a detailed investigation of a simple poppet valve and he deduced a stability criterion analytically. He also showed that effects other than fluid nonlinearity can lead to stability loss, such as changes in the poppet geometry or the oil temperature. Moreover he performed experiments and found good coincidence with his analytical results. Thomann [15] was also interested in the analysis of a pipe-valve system. He used a simple poppet type valve but analysed how different poppet geometries affect the stability. He investigated a conical and a cylindrical poppet together with conical or cylindrical seats, and their combination. Hayashi et al.[8, 9], built up a model with a constant supply pressure and investigated the valve's response and stability, finding that the point of instability can be characterised as a Hopf bifurcation.

The purpose of this paper is to go beyond the initial instability and to explain the dynamics that occurs when the valve starts to chatter, that is, where the poppet starts to periodically impact with the valve seat. Recent progress in nonsmooth dynamical systems has enabled analysis and simulation techniques to capture such behaviour, see [3] and references therein. These techniques were recently applied by Eyres et al. [5, 6] to a model of a hydraulic motion damper with relief valves that are present to achieve certain bilinear damping characteristics. Complex dynamics in that system were explained by the presence of grazing impact within the valves.

This article is organised as follows. In Section 2 a simple mathematical model is derived that is inspired by recent experimental results on a test valve embedded within a simple hydraulic circuit. The model incorporates fluid compressibility and Newtonian restitution to model the impact between the valve poppet and seat and can be shown to depend on four dimensionless parameters. Section 3 presents a linear and nonlinear analysis of the initial instability of the model. Section 4 goes on to study the more global dynamics for a particular set of parameters for which there is an interval of flow speeds in which the valve undergoes self-excited oscillations. The complex nonlinear dynamics observed for these flow speeds is then explained using the theory of grazing bifurcations. Section 5 sums up the results.

*Department of Applied Mechanics, Budapest University of Technology and Economics, licsko@mm.bme.hu
†Department of Engineering Mathematics, University of Bristol, A.R.Champneys@bristol.ac.uk
‡Department of Hydrodynamic Systems, Budapest University of Technology and Economics, csaba.hos@hds.bme.hu

2 The mathematical model

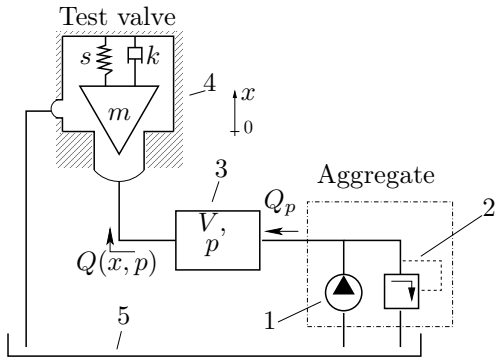

Figure 1: Schematic diagram of a simple hydraulic system consisting of a gear pump (1), a relief valve (2), a hypothetical chamber (3) that represents the total tubing in a real system, an oil tank (5) and the pressure relief valve (4) that we wish to test.

Figure 1 depicts the schematic layout of an experimental hydraulic rig that is designed to test the behaviour of a pressure release valve. Preliminary experimental data for this rig has indicated the propensity of the valve to self-oscillate at around 300-400 Hz for a range of flow speeds and for there to be significant hysteresis between the self-oscillating and the equilibrium states [13]. The details of these experiments will appear elsewhere.

In order to derive a mathematical model of the system we embed a similar model of the value to that used by Kasai [10] and Hayashi [9] within a simple mass flux model for the fluid, whose flow we suppose to be supplied at a constant rate Q_p by a gear pump (labelled 1 in Fig. 1). However due to compressibility of the fluid and elasticity of the tubes, the flow rate at the test valve can be different from that at the exit of the pump. So we consider a hypothetical chamber whose volume is equal to the total volume of the system when filled with oil, within which we allow a flow rate difference between the inlet and the outlet. This chamber will represent the stiffness of our system.

The mass balance equation for the chamber (labelled 3 in Fig. 1) can be written as follows:

$$\frac{d}{dt}(\rho V) = V\frac{\rho}{E}\frac{dp}{dt} = \rho\left[Q_p - Q(x,p)\right], \tag{1}$$

where V represents the total volume of the system, ρ denotes the density of the fluid and p is the oil pressure at the relief valve. Furthermore, the term

$$Q(x,p) = A(x)C_d\sqrt{\frac{2}{\rho}p} \tag{2}$$

is the flow rate of the fluid leaving the valve, where C_d (which in general depends on Reynolds number Re, although here we take to be constant) is the discharge coefficient at the valve inlet. Also, $A(x)$ is the cross sectional area of the valve inlet, where x is the displacement of the valve stem, which is zero when the valve is closed and positive otherwise. In general, an accurate expression for the orifice cross-sectional area as a function of the value displacement $A(x)$ will be nonlinear and will depend on the precise valve geometry. Nevertheless, since during most operations, the valve displacements will be small it is reasonable to linearise and write $A(x) = A_1 x$. In practice any nonlinearity due to the valve geometry is likely to be small compared with that due to fluid compressibility and to the impact. Note that in deriving (1) we have used the chain rule for derivatives and also substituted $\frac{dp}{d\rho} = \frac{E}{\rho}$ as a definition for the sonic speed, where E is the reduced modulus of elasticity of the system after taking account of the oil compressibility and the expansion of the tubes.

The equation of motion for the valve poppet is assumed to take the form:

$$\begin{aligned}\dot{x} =& v\\ \dot{v} =& \frac{pA}{m} - \frac{k}{m}v - \frac{s}{m}(x + x_0)\end{aligned} \tag{3}$$

for $x > 0$, and to obey a Newtonian impact law

$$v^+ = R\left(v^-\right) = -rv^- \tag{4}$$

when $x = 0$. Here v denotes the velocity of the valve stem, with v^- being its value immediately before an impact, and v^+ its value immediately afterwards, r is the coefficient of restitution, k is the valve's damping coefficient when not in contact, s is the spring stiffness, m is the total mass of the moving parts and x_0 denotes the pre-compression of the spring.

Introducing the dimensionless co-ordinates $y_i(\tau)$, $i = 1, 2, 3$ where

$$\tau = (\frac{s}{m})^{\frac{1}{2}}t, \quad y_1 = \frac{s}{A_0 p_0}x, \quad y_2 = \frac{(sm)^{\frac{1}{2}}}{A_0 p_0}v, \quad y_3 = \frac{1}{p_0}p\,,$$

where p_0 is atmospheric pressure, A_0 is the inlet cross sectional area of the valve, Eqns. (1)–(4) can be written in dimensionless form as

$$\begin{aligned}y_1' &= y_2\\ y_2' &= -\kappa y_2 - (y_1 + \delta) + y_3\\ y_3' &= \beta\left(q - \sqrt{y_3}y_1\right)\end{aligned} \tag{5}$$

for $y_1 > 0$, where $'$ represents differentiation with respect to τ, and

$$y_1^+ = -ry_1^-\,.$$

for $y_1 = 0$. The nondimensional parameters are

$$\kappa = \frac{k}{m}\sqrt{\frac{m}{s}} \text{ (nondimensional damping coefficient)}$$
$$\beta = \frac{E}{V}\frac{C_d A_1 A_0}{\rho}\sqrt{\frac{2p_0 m}{\rho s}} \text{ (nondim. stiffness param.)}$$
$$\delta = \frac{s x_p}{A_0 p_0} \text{ (nondimensional pre-stress parameter)}$$
$$q = \frac{Q_p}{C_d c_1 \frac{A_0 p_0}{s}\sqrt{2\frac{p_0}{\rho}}} \text{ (nondimensional flow rate).}$$

We use experimental test rig [13] to estimate realistic values for the dimensionless parameters. We obtain that

$$\kappa \approx 1.25\,[-], \qquad \beta \approx 20\,[-], \quad \text{and} \quad \delta = 10\,[-], \tag{6}$$

which corresponds to an opening pressure for the relief valve of $p_{opening} = 10\,[bar]$. The dimensionless flow rates are allowed to vary in the range $0-25$, which corresponds to Q_p in the range $0-3.5\,[l/\text{min}]$. Of these parameters the nondimensional damping coefficient is the one that carries the most uncertainty as it is the hardest to approximate in practice.

3 Initial instability

Throughout this section, we take the simplifying assumption that that there is no pre-stress in the valve, $\delta = 0$ (which is not as gross a simplification as it might seem since the average pressure p also acts like a pre-stress term). Moreover in numerical evaluations we take the dimensionless stiffness parameter $\beta = 1$. These simplifications make the analysis somewhat more tractable, and in practice was found to make little qualitative difference; an effective adjustment can be made by reducing κ to about 0.7.

3.1 Linear stability analysis

Under the assumption $\delta = 0$, the equilibrium of Eq. (5) is

$$(y_1^e, y_2^e, y_3^e) = (q^{\frac{2}{3}}, 0, q^{\frac{2}{3}}).$$

Linear stability analysis shows that a Hopf bifurcation (corresponding to a pure imaginary pair of eigenvalues) occurs along a curve in the (κ, q) parameter plane given by

$$\kappa = \frac{-\beta^2 q^{\frac{2}{3}} - 4 + \sqrt{\beta^4 q^{\frac{4}{3}} + 40\beta^2 q^{\frac{2}{3}} + 16}}{4\beta q^{\frac{1}{3}}}. \tag{7}$$

Figure 2(a) shows this curve. For higher κ values the system becomes unstable to linear oscillations. We can also calculate the frequency of small amplitude oscillations, which is depicted as a function of κ in Fig. 2(b) in the original dimensional co-ordinates. Note that this frequency of instability is found to be remarkably constant along the curve, at approximately 314Hz, which is within the range observed in the experiments.

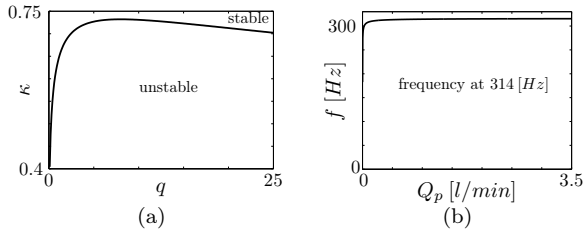

Figure 2: (a) Stability diagram for the nondimensional damping coefficient κ with respect to the nondimensional flow rate q under the simplifying assumptions $\delta = 0$, $\beta = 1$. (b) The corresponding vibration as a function of flow rate, using the dimensional parameters derived from the test rig.

3.2 Nonlinear analysis

Having found the presence of a Hopf bifurcation, let us next investigate the stability of the bifurcating limit cycle. We have applied the technique of centre manifold reduction and normal form theory as described for example in [7, 12]. The normal form for a Hopf bifurcation on the centre manifold can be written in the complex form

$$\dot{z} = (\lambda + i\omega)z + l_1 z|z|^2 + O(z^5),$$

where λ gives the real part of the eigenvalues that cross the imaginary axis at the bifurcation and ω their imaginary parts. The sign of the *first Lyapunov coefficient* l_1 determines the criticality of the Hopf bifurcation. That is, if $l_1 < 0$ small-amplitude limit cycle oscillations bifurcate supercritically (stable oscillations for $\lambda > 0$), whereas for $l_1 > 0$ they bifurcate subcritically (unstable oscillations for $\lambda < 0$).

We have computed the Lyapunov coefficient at all points along the instability curve in Fig. 2(a), see Fig. 3. Indeed, note from the middle panel of the figure that l_1 changes sign at some point along the curve. In fact, the coefficient changes sign at precisely $\chi = 3.4087\,[-]$ where $\chi = \beta q^{1/3} \sim q$ is a convenient combination of dimensionless parameters.

Taking the specific case $\kappa = 0.7$, Fig. 3 shows that both Hopf points are supercritical, since $l_1 < 0$. This means that the limit cycle that arises at the Hopf points will be stable. However if we reduce κ, then the two bifurcation points move apart and one of them becomes subcritical. In order to understand these cases and provide verification of the analysis, we have used the public domain software AUTO [4] to continue the limit cycles as parameters vary. Figure 4 shows the numerical continuation with $\kappa = 0.7$, where there are two supercritical Hopf bifurcation points. The solid lines represent the data from

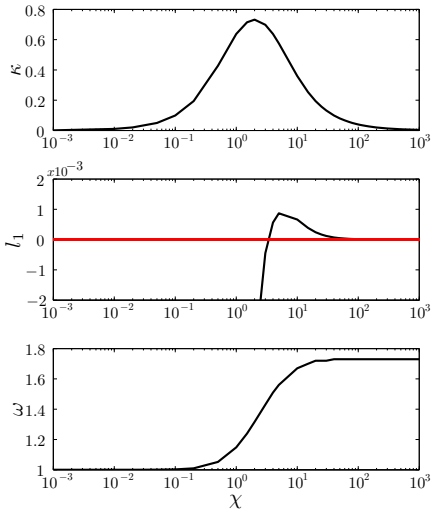

Figure 3: Stability curve (top), values of the Lyapunov coefficient along the stability curve (middle) and the nondimensional vibration frequency (bottom) against $\chi = q^{1/3}\beta$, plot on a logarithmic scale

the AUTO calculation and the dashed lines show the analytical estimates for the vibration amplitude which can be obtained from the cubic-order normal form. Note that

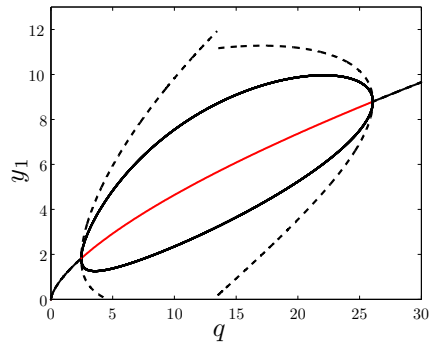

Figure 4: Continuation of equilibria and limit cycles with q for $\kappa = 0.7$. The dashed lines represent the analytical estimates, and the solid lines the results of AUTO computation. The approximately straight line represents the curve of equilibria, which is unstable between the two Hopf bifurcation. The curves that bifurcate at the two Hopf points represent the maximum amplitude and minimum amplitude of a limit cycle, which is stable for all the depicted q-values.

for this κ-value the auto computations show that a stable limit cycle exists throughout the region between the two Hopf bifurcation points. Moreover this limit cycle has a minimum amplitude for which y_1 is positive, hence no impacts occur.

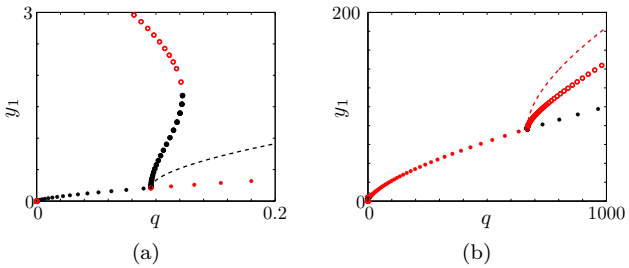

Figure 5: Continuation from Hopf bifurcation points with $\kappa = 0.4$ showing: (a) a neighbourhood of the first, supercritical, Hopf bifurcation; (b) a neighbourhood of the second, subcritical, bifurcation. Here stars mark the location of equilibria and circles represent periodic solutions. Black markers are stable solutions and red ones are unstable. The dashed line again shows the analytical estimation from the normal form theory which can be seen to be quadratically correct.

It is interesting to compare these results with what happens when κ is reduced to a value of 0.4. Again Fig. 3 shows that there are two Hopf bifurcation points, but now the higher-q one (at the unphysically large value of $q = 668.2$) is subcritical, while the lower q bifurcation (at $q = 0.096$) remains supercritical. However, the results in Fig. 5(a) show that the bifurcating limit cycle from the supercritical bifurcation only exists for a short interval of q-values before it destabilises in a fold of limit cycles. This unstable limit cycle exists all the way down to $q = 0$. Fig. 5(b) shows continuation from the second Hopf point at $q = 668.2$. The unstable limit cycle born in this bifurcation can be continued up to arbitrarily large q.

For this lower κ-value then we have found a large interval of q parameters for which there are no stable dynamics arising from the solutions born at the Hopf bifurcations. To understand what happens for these flow speeds, we must turn to direct numerical simulation.

4 Global dynamics

We now return to the original experimentally determined values of the fixed parameters (6) in order to investigate the dynamics well away from the initial Hopf instability.

4.1 Direct numerical simulation

In order to determine the long-time dynamics for any parameter value we have performed numerical simulation of the dimensionless model (5) using MATLAB® and the *event handling* solver option to accurately detect impact points where $y_1 = 0$. If an impact occurs at a point $y = y^-(0, v^-, p^-)^T$ then a *reset map* is applied so that the new initial condition becomes $y^+ = (0, -rv^+, p^+)^T$.

We vary the nondimensional flow rate q as free parame-

ter in order to produce a so called *Monte Carlo* bifurcation diagram, in which we take a range of different initial conditions at each q-value then run the simulation for a long time, recording points only after transients have died. In order to depict the results, we chose the plane $\{y_2 = 0\}$ as a two-dimensional *Poincarè section* of the three-dimensional phase space. The results are presented in Fig. 6.

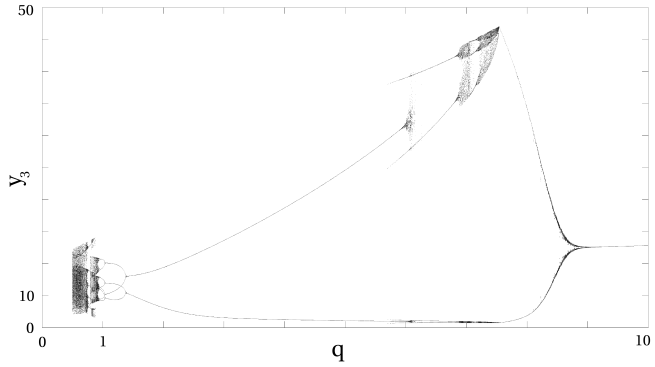

Figure 6: Monte Carlo bifurcation diagram for $\kappa = 1.25$, $\beta = 20$, $\delta = 10$ and $q = 0 - 10$.

There are some interesting regions in the figure that are worthy of discussion. Let us consider reducing q from a high value towards zero. At about $q = 9.18$ a supercritical Hopf bifurcation occurs and a stable limit cycle is born that rapidly grows in amplitude with further decrease of the bifurcation parameter. This extreme growth can be explained from the fact that the first Lyapunov coefficient remains relative close to zero but is clearly negative for these particular parameter values of q. A typical solution trajectory within this region is depicted in Figure 7(a).

At $q \cong 7.54$ a *grazing bifurcation* occurs. This means that the minimum value of the vibration reduces until it reaches the impacting barrier $y_1 = 0$, which means that the displacement x of the valve poppet has reached 0, the value at the valve seat in our physical system. At grazing, only zero velocity impacts occur, this also means that the reset map that is used for determining the velocity after impact is the identity map itself, the velocity before and after the impact are both equal to zero.

With further decrease of the dimensionless flow rate, period-three and period-two impacting solutions can be seen between $q = 6.1$ and 7.54. Parts of this region seem to be cloudy which is the hallmark of chaotic motion. Figure 7(b) shows an impacting (weakly) chaotic solution.

The next interesting point is at $q \cong 5.9$ where a period-two and a period-one impacting solution coexist. The period-two solution is an impacting/grazing one that can be seen in Figure 7(c). This also suggests that another grazing bifurcation occurs in this region when the non-

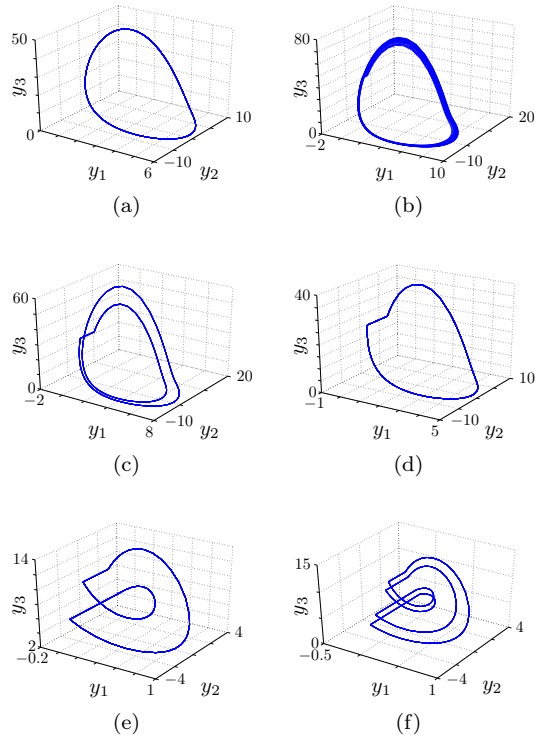

Figure 7: Phase space trajectories along the bifurcation diagram: (a) Non-impacting period-one ($q = 8$); (b) near-grazing chaotic orbit ($q = 7.4$); (c) period-two impacting ($q = 6.5$); (d) period-one impacting ($q = 5$); (e) period-two impacting ($q = 1.2$); (f) period-four impacting ($q = 1$). The parameters are $\kappa = 1.25$, $\beta = 20$ and $\delta = 10$.

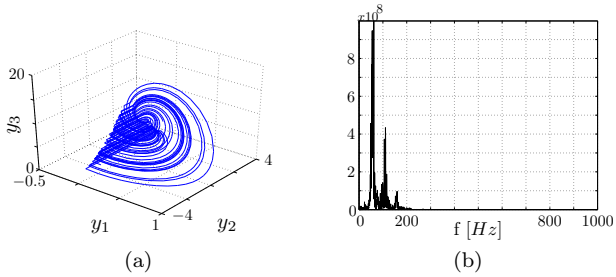

Figure 8: (a) Chaotic attractor for $q \approx 0.85$ with $\kappa = 1.25$, $\beta = 20$ and $\delta = 10$. (b) The frequency spectrum of the solution.

impacting period of the period-two solution touches the impact surface. Below $q = 5.7$ only a period-one impacting solution exists until $q = 1.4$ where a so called period-doubling cascade starts Figures 7(d), 7(e) and 7(f) show trajectories corresponding to this region. This period-doubling cascade ends up in the chaos that can be seen on Fig. 8(a) and Fig. 8(b).

4.2 Grazing bifurcation analysis

In our system for the particular nondimensional parameters used (6), grazing can occur at the two flow-rates $q = 7.54$ (henceforth referred to as the *first* grazing) and $q = 5.95$ (the *second* one). The first grazing occurs when the period-one nonimpacting limit cycle depicted in Fig. 7(a) touches the impact barrier. The second grazing is when a period-two limit cycle that already has an impacting period undergoes another point of grazing (see Fig. 7(c)). In both cases this is characterised by the appearance of a zero velocity impact, however the two grazing events have different effects on the global dynamics. In the first case an immediate jump to chaos can be seen (see Fig. 9(a)) while the second case looks more complicated as depicted in Fig. 9(b).

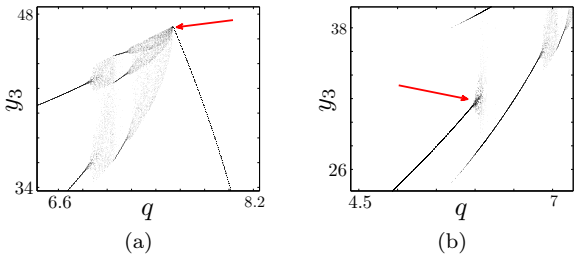

Figure 9: Two grazing events shown in the bifurcation diagram. The first at $q = 7.54$ (a) and the second at $q = 5.95$ (b).

We have carried out a more detailed investigation of the first grazing, in order to understand the apparent immediate transition to chaotic dynamics. For this we used the theory for nonsmooth systems described in [3]. First we have to find the grazing limit cycle exactly. Our bifurcation diagram in Fig.6 is very helpful, because it contains the critical flow rate q and the nondimensional pressure y_3 can also be obtained. Since we chose the zero velocity plane as our Poincarè section $y_2 = 0$ and at grazing our displacement is also zero. We now have initial conditions that correspond to the last non-impacting limit cycle. The next step is to solve the linear variational equations along the limit cycle at the grazing point, to obtain the *monodromy matrix* M whose eigenvalues are the Floquet multipliers of the orbit. The variational equations can be written in the form

$$\dot{w} = \hat{J}(y_0)w, \tag{8}$$

where $\hat{J}$ is the linear part of the nonlinear system defined in Eq.(5) evaluated along the impacting orbit y_0. We have to solve (8) together with (5) over the period T of the grazing limit cycle. To compute a basis for M, we need to solve (8) with three different initial conditions $\left(w_1^{01}, w_2^{01}, w_3^{01}\right) = (1,0,0)$, $(0,1,0)$ and $(0,0,1)$. We can then form the monodromy matrix M from the solution $w(T)$ after one complete period:

$$M = \left(w^{01}(T)\, w^{02}(T)\, w^{03}(T)\right).$$

We then have to compute the eigenvalues of M in order to apply the theory of grazing bifurcations.

Since the grazing limit cycle is stable, the eigenvalues of M (apart from the trivial multiplier 1) must both lie inside in the unit circle. If these eigenvalues $\nu_{1,2}$ are both real, then generically we may assume $|\nu_1| > |\nu_2|$ and, according to theory in [3] there are three scenarios:

1. If $0 < |\nu_1| < 1/4$ then grazing is followed by a period adding cascade, in which overlapping parameter intervals exist in which there is an orbit of period nT, where $n \to \infty$ as the grazing point is approached;
2. if $1/4 < |\nu_1| < 2/3$ then chaotic and stable periodic solutions alternate and the periodic motion forms a period adding cascade;
3. if $2/3 < |\nu_1| < 1$ then there is a sudden jump to chaos where the chaotic attractor's size is proportional to the square root of the bifurcation parameter.

For the grazing flow rate $q = 7.54$ we find that $\left(y_1^0, y_2^0, y_3^0\right) = (0, 0, 47.07)$ represents the initial condition of a periodic orbit that grazes. When we integrate for one period ($T = 2.6547\,[-]$ for this flow rate) and solve the linear variational equations we obtain that the nontrivial eigenvalues of M are $\nu_1 = 0.8537$ and $\nu_2 \approx 0$. Since we have $2/3 < \nu_1 < 1$, the above classification shows that a robust chaotic attractor should be born at the bifurcation, whose size grows with $\sqrt{7.54 - q}$. This is exactly as seen in Fig. 9(a). The second grazing bifurcation at $q = 5.95$ can be analysed similarly, but here the computations are more involved, since the periodic orbit undergoing the bifurcation is itself an impacting one.

5 Conclusions

In this paper we presented a mathematical analysis of a simple hydraulic pressure relief valve. We found that these kind of dynamical systems can lose their stability in a particular way in which self-excited limit cycle vibrations occur. We obtained a criterion for stability regarding the flow rate and damping coefficient parameters using linear stability analysis. We have shown that damping of the system has a notable effect on the stability of limit cycles that arises. Overall, an increase of damping κ makes the system more stable, and if the damping is moderate but not too small, it can help to avoid the appearance of unstable limit cycles.

We also found that for low enough damping, the system typically undergoes grazing bifurcations at two flow rates and we determined the type of grazing bifurcation that

causes the initial onset of impacting behaviour as the flow rate is decreased. We were able to show that this causes a transition from a stable limit cycle to robust chaos. We believe this is the first proper explanation of the onset of chattering behaviour in relief valves, as most previous studies have assumed smooth behaviour, and essentially has just found the presence of Hopf bifurcations. As we have shown, an analysis of chatter requires instead non-smooth dynamical systems theory.

This work is part of an ongoing wider study, and a detailed comparison between theory and experiment will be discussed elsewhere. It is also planned to do further parametric studies, in particular implementing continuation that take account of the system's discontinuity.

References

[1] W. Bolton. *Pneumatic and hydraulic systems*. Butterworth-Heinemann, 1997.

[2] B. Brogliato. *Impacts in Mechanical Systems – Analysis and Modelling*. Springer–Verlag, New York, 2000. Lecture Notes in Physics, Volume 551.

[3] M. di Bernardo, C. J. Budd, A. R. Champneys, and P. Kowalczyk. *Piecewise-smooth dynamical systems*. Springer, 2007.

[4] E. J. Doedel. *AUTO-07P : Continuation and Bifurcation Software for Ordinary Differential Equations*. Technical manual.

[5] R. D. Eyres, A. R. Champneys, and N. A. J. Lieven. Modelling and dynamic response of a damper with relief valve. *Nonlinear Dynamics*, (40):119–147, 2005.

[6] R. D. Eyres, P. T. Piiroinen, A. R. Champneys, and N. A. J. Lieven. Grazing bifurcations and chaos in the dynamics of a hydraulic damper with relief valves. *SIAM Journal on Applied Dynamical Systems*, 4(4):1076–1106, 2005.

[7] J. Guckenheimer and P. Holmes. *Nonlinear oscillations, dynamical systems, and bifurcations of vector fields*. Springer, 1983.

[8] S. Hayashi. Instability of poppet valve circuit. *JSME International Journal*, 38(3), 1995.

[9] S. Hayashi, T. Hayase, and T. Kurahashi. Chaos in a hydraulic control valve. *Journal of fluids and structures*, (11):693–716, 1997.

[10] K. Kasai. On the stability of a poppet valve with an elastic support. *Bulletin of JSME*, 11(48), 1968.

[11] F. X. Kay. *Pneumatics for industry*. The Machinery Publishing Co. Ltd., 1959.

[12] Yuri A. Kuznetsov. *Elements of applied bifurcation theory*. Springer, 1997.

[13] Gábor Licskó. Nonlinear analysis of a hidraulic pressure relief valve. Master's thesis, Budapest University of Technology and Economics, 2008.

[14] H. L. Stewart. *Hydraulic and pneumatic power for production*. The Industrial Press, 1963.

[15] H. Thomann. Oscillations of a simple valve connected to a pipe. *Journal of Applied Mathematics and Physics*, 1976.

[16] M. Wiercigroch and B. de Kraker. *Applied Nonlinear Dynamics and Chaos of Mechanical Systems with Discontinuities*. World Scientific Publishing, 2000.